

¹ RG-D COMMON ANALYSIS NOTE

² ELECTRON AND PION CUTS FOR RUN GROUP D

³ MATHIEU OUILLON

⁴ *Mississippi State University*

⁵

⁶ ouillon@jlab.org

7 Contents

8	1	Particle identification and fiducial cuts	1
9	1.1	Electron identification	1
10	1.2	Electron fiducial cuts	9
11	1.2.1	Calorimeters fiducial cuts	9
12	1.2.2	DC fiducial cuts	10
13	2	Summary	14
14	A	Sector Parameters	16
15	B	Number of photo-electrons in HTCC	17
16	C	Sampling fraction versus momentum	17
17	D	Calorimeter fiducial cuts	17

18 SECTION 1

19

Particle identification and fiducial cuts

20

21 In this section, we detail the particle identification and selection using
 22 the CLAS12 detector. We focus on the measurement of electrons in the
 23 forward detector and charged pions in the forward and central detectors.
 24 Particle identification and refined selection follow procedures developed by
 25 Run Group A.

26 Data has been taken from Pass1 with a beam energy of 10.54 GeV and
 27 has been produced with CLAS12 software [COATJAVA 13.0.0](#). The data
 28 are available at </cache/clas12/rg-d/production/Pass1/>.

29 SUBSECTION 1.1

30

Electron identification

31

32 The electron is typically the first particle required to define an event for
 33 physics analysis. To accurately identify electron candidates, a series of
 34 selection criteria, or cuts, is applied to detector responses, specifically
 35 targeting negatively charged tracks. These cuts are designed to distin-
 36 guish electrons from minimum ionizing particles (MIPs), such as negatively
 37 charged pions (π^-). Additionally, the Event Builder assigns a classification
 38 (**status**) based on the detector system in which the electron track is lo-
 39 cated.

40 In the initial step, the Event Builder assigns electron or positron identi-
 41 fication ($e^- \rightarrow 11, e^+ \rightarrow -11$) to tracks that exhibit appropriate responses
 42 in both the High Threshold Cherenkov Counter (HTCC) and the Electro-
 43 magnetic Calorimeter (ECAL), following the criteria outlined in table 1.
 44 Additionally, the EB requires an associated matched hit in FTOF, either
 45 in panel-1b or, if there is no panel-b hit, in panel-1a.

Cut	Requirement	Purpose
Charge	$Q = -1$	Select negative tracks
HTCC Photoelectrons	$N_{\text{phe}} > 2$	Reject charged hadrons
PCAL Energy	$E_{\text{PCal}} > 60 \text{ MeV}$	Reject MIPs
Sampling Fraction	$\pm 5\sigma$ vs $E_{\text{Tot,dep}}$	Electromagnetic shower identification
Track Matching	Geometric matching	Ensure correct track

Table 1. EB electron (`pid = 11`) assignment requirements. The EB sampling fraction is parameterized based as a function of the total energy deposited in the calorimeters. Electrons defining the event start time are prioritized to the first column of the `REC::Particle` data structure (bank) and have a negative status.

46 Since CLAS12 can detect particles across a broad kinematic range,
 47 electron detection is restricted to the Forward Detector. This restriction is
 48 implemented by selecting events with a negative status in the range (-4000,
 49 -2000]. A negative status indicates that the track contributed to the event
 50 trigger. The particle status reflects the detector topology and is determined
 51 by summing the numerical values assigned to individual detector hits:

$$\text{status} = 1000 \times \text{FT} + 2000 \times \text{FD} + 4000 \times \text{CD} + 100 \times N_{\text{scint}} + 10 \times N_{\text{cal}} + 1 \times N_{\text{cher}}$$

52 With the FT subsystem being 1 if used, else 0, same for CD and FD for
 53 the central subsystem and forward subsystem, respectively.

54 The charge of a particle determines its curvature as it moves through
 55 the toroidal magnetic field. Depending on the field polarity, particles expe-
 56 rience inbending or outbending deflections along the polar angle. Electrons,
 57 being negatively charged, bend inwardly during inbending configurations
 58 and outwardly during outbending configurations.

59 The High Threshold Cherenkov Counter (HTCC) is used to minimize
 60 negative pion contamination in electron samples for candidate tracks below
 61 4.5 GeV momentum. Below this momentum threshold, selecting electrons
 62 based on the number of detected photo-electrons (N_{phe}) is sufficient. Elec-
 63 tron candidate tracks produce more than 2 photo-electrons (see fig. 1 and
 64 fig. 18).

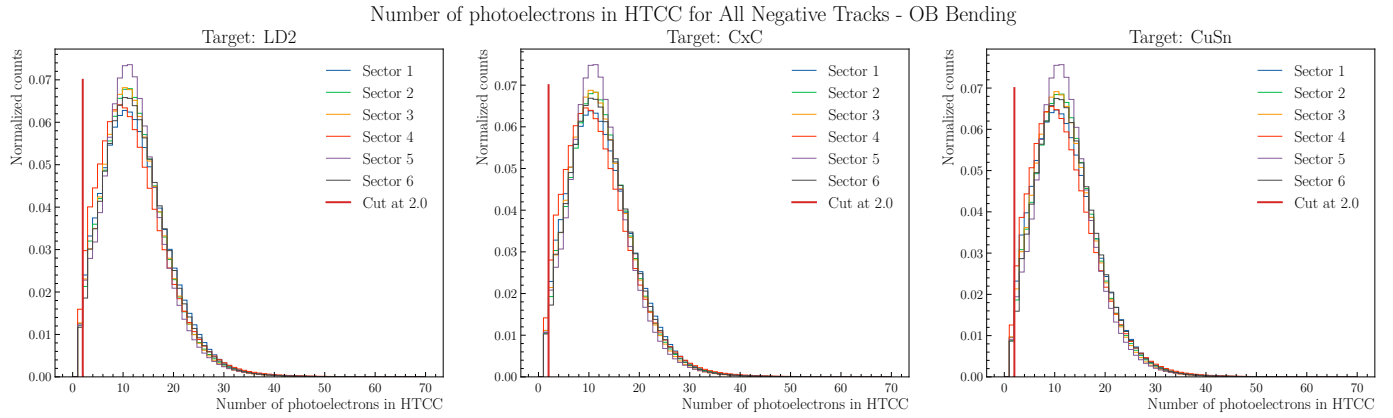


Figure 1. HTCC photo-electron distribution for all negative tracks in the Forward Detector in outbending polarity for the torus, apply cut at $N_{\text{phe}} > 2$ for pion rejection.

65 Two calorimetric cuts discriminate between electrons and minimum
 66 ionizing particles (MIPs), primarily negative pions. The first cut utilizes
 67 energy deposition in the preshower calorimeter (PCAL) and electromag-
 68 netic calorimeter (ECAL), with the latter divided into inner and outer
 69 regions. Electrons develop extended electromagnetic showers and deposit
 70 significant energy, while pions deposit consistently lower energy as MIPs.

- 71 This distinct energy signature enables electron selection through a 0.06
 72 GeV threshold cut, rejecting pions below this value (see fig. 2).

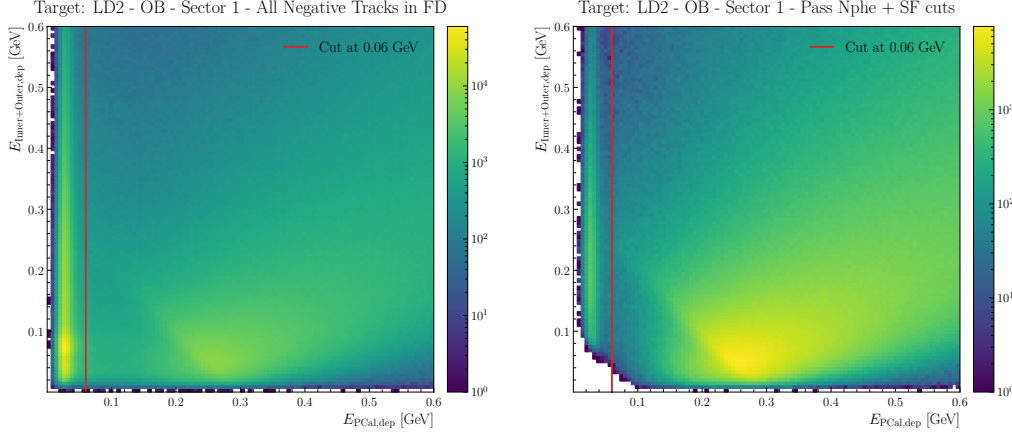


Figure 2. PCAL minimum energy cut $E_{\text{PCal,dep}} > 60$ MeV (black line), for sector 1, to remove pions. (a) All negative tracks. (b) Negative tracks which pass the conditions on the number of photoelectrons in the HTCC and on the sampling fraction in the calorimeter.

73 In the RG-A Common Analysis Note, a fixed threshold of 0.07 GeV was
 74 used for the PCAL energy cut. However, as shown in fig. 3, this threshold
 75 was found to be too high for RG-D, leading to the exclusion of valid electron
 76 tracks. Indeed a cut a 0.06 GeV is already equivalent to a 7σ cut on the
 77 PCAL energy distribution for π^- . The σ have been obtained by fitting
 78 with a Gaussian the top of the peak of the PCal energy distribution after
 79 the N_{phe} and SF cuts.

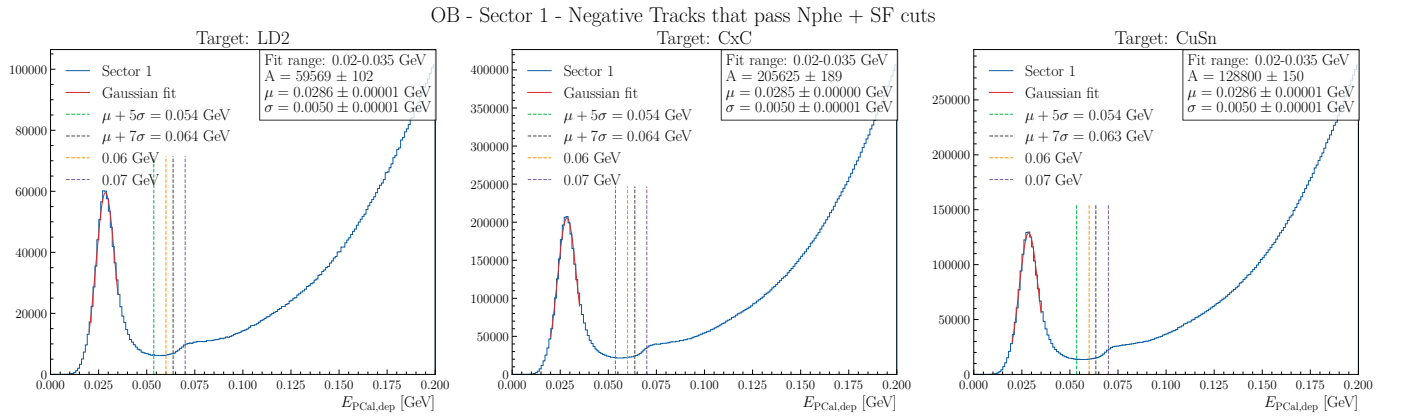


Figure 3. PCAL minimum energy cut $E_{\text{PCal,dep}} > 70$ MeV (purple line) used in RG-A, for sector 1, to remove pions. The orange line is the 7σ cut on the PCAL energy distribution for π^- .

In addition to the minimum PCAL energy threshold cut, a sampling fraction cut is applied to further eliminate negative pion tracks. The sampling fraction is defined as the ratio of the total deposited energy $E_{\text{dep},\text{Total}} = E_{\text{dep,PCAL}} + E_{\text{dep,ECAL,Inner}} + E_{\text{dep,ECAL,Outer}}$ to the reconstructed track momentum p . For electrons, this fraction remains nearly constant at ~ 0.25 across all momenta, indicating that the deposited energy scales proportionally with the electron's momentum. In contrast, negative pions, as minimum ionizing particles (MIPs), deposit a relatively constant amount of energy regardless of momentum. To accurately select electrons, tracks are required to be within $\pm 5\sigma$ of the sampling fraction as a function of total deposited energy. This is achieved by binning the data in $E_{\text{Tot,dep}}$, fitting a Gaussian to the sampling fraction distribution in each bin to extract the mean (μ_b) and standard deviation (σ_b), and then parameterizing these values using eq. (1.2). The resulting functions define the energy-dependent sampling fraction cut.

$$\mu_{\text{SF}} = a(b + c/E_{\text{Tot,dep}} + d/E_{\text{Tot,dep}}^2) \quad (1.1)$$

$$\sigma_{\text{SF}} = e(b + f/E_{\text{Tot,dep}} + g/E_{\text{Tot,dep}}^2) \quad (1.2)$$

The parameters a, b, c, d, e, f and g can be found in the CCDB for EB.

The electron tracks are selected $\pm 5\sigma$ from the sampling fraction as a function of the $E_{\text{Tot,dep}}$. as seen in fig. 4.

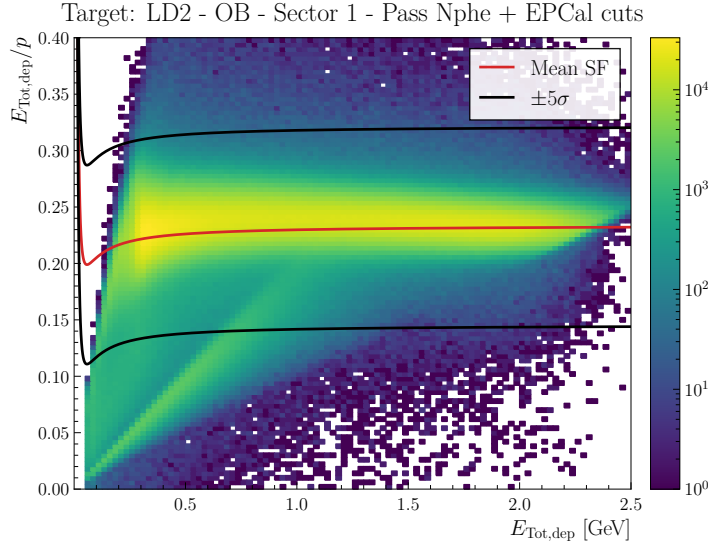


Figure 4. Sampling fraction, the ratio of the sum of energy deposited in the calorimeter layers to reconstructed track momentum, vs deposited energy for each pre-shower calorimeter sector. The electron candidate tracks shown are with the N_{phe} and E_{PCal} cuts applied. The red line is the result of the fit to the mean, and black lines are at $\pm 5\sigma$.

$$SF = \frac{E_{\text{PCAL,dep}} + E_{\text{Inner,dep}} + E_{\text{Outer,dep}}}{p} \quad (1.3)$$

To improve the electron identification, another cut on the sampling fraction as a function of the momentum has been developed. For that, the SF is binned in momentum, and the resulting SF distribution is fit with a Gaussian distribution to extract the mean and sigma for a given momentum range. The momentum or energy dependence of the mean and sigma can then be fit to eq. (1.5)

$$\mu_{\text{SF}} = a_\mu + b_\mu p + c_\mu p^2 + d_\mu p^3 \quad (1.4)$$

$$\sigma_{\text{SF}} = a_\sigma + b_\sigma p + c_\sigma p^2 + d_\sigma p^3 \quad (1.5)$$

The cut is then defined as $\mu_{\text{SF}} + 3\sigma_{\text{SF}}$ as seen in fig. 5b for the carbon target, in fig. 5a for the LD2 target, and in fig. 5c for the copper and tin target (CuSn). The fits to the SF mean function are given in red line and the sigma function upper and lower limits as a black line.

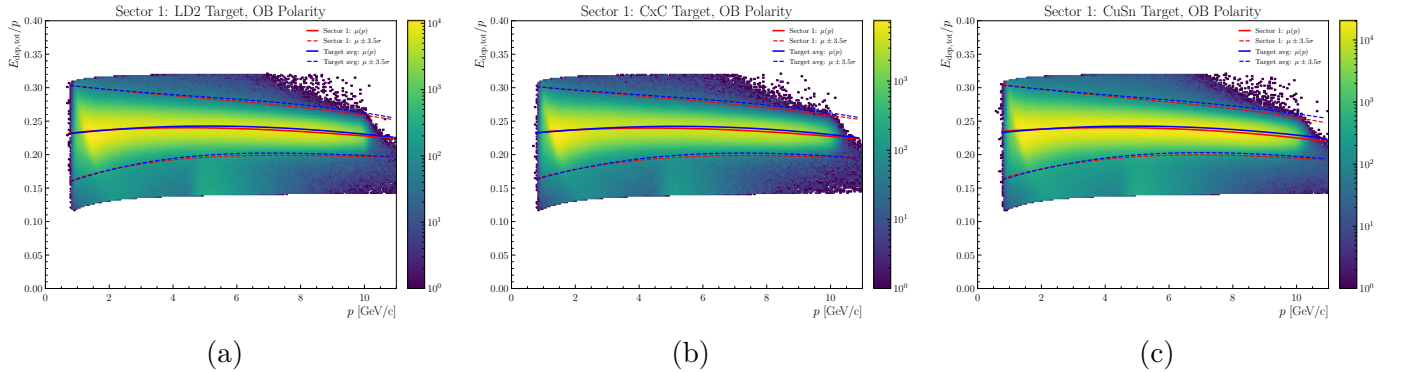


Figure 5. Sampling fraction vs momentum for electron candidate tracks in outbending polarity for different targets: (a) LD2, (b) carbon, and (c) copper and tin (CuSn). The red lines is the fit to the mean and the $\pm 3.5\sigma$ for the sector 1. The blue lines are the same fit but for the sector average.

This cut is obtained by slicing the SF distribution in 50 momentum bins from 0 to 11 GeV, fitting the peak from half of the height on the left to half of the height on the right with a Gaussian to each slice to extract the mean and sigma, and then fitting these values to eq. (1.5).

The plot in fig. 6 shows a comparison between the sampling fraction mean and standard deviation as a function of momentum for the LD2 target in outbending polarity for different sectors and the overall distribution. The same plots are available for the CxC and CuSn targets in the appendix.

The fig. 7 shows a comparison between the sampling fraction mean and standard deviation as a function of momentum for all the targets in outbending polarity for the average over all sectors.

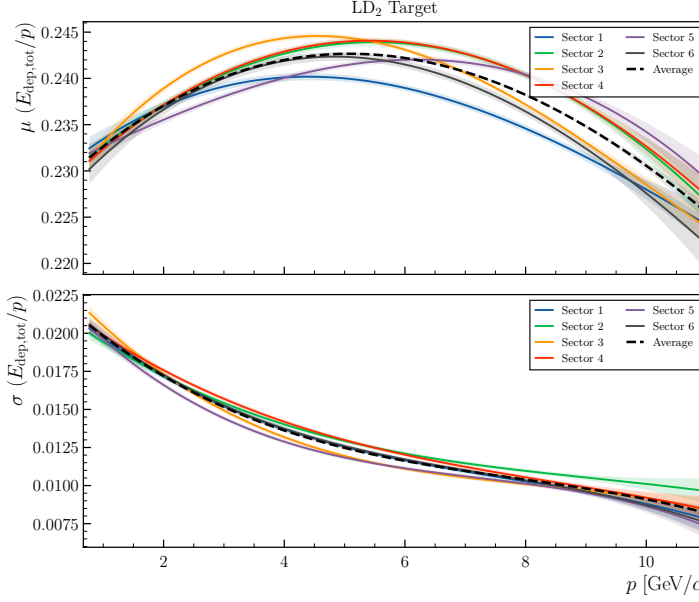


Figure 6. Comparison of the sampling fraction mean and sigma as a function of momentum for the LD2 target in outbending polarity for different sectors and the overall distribution.

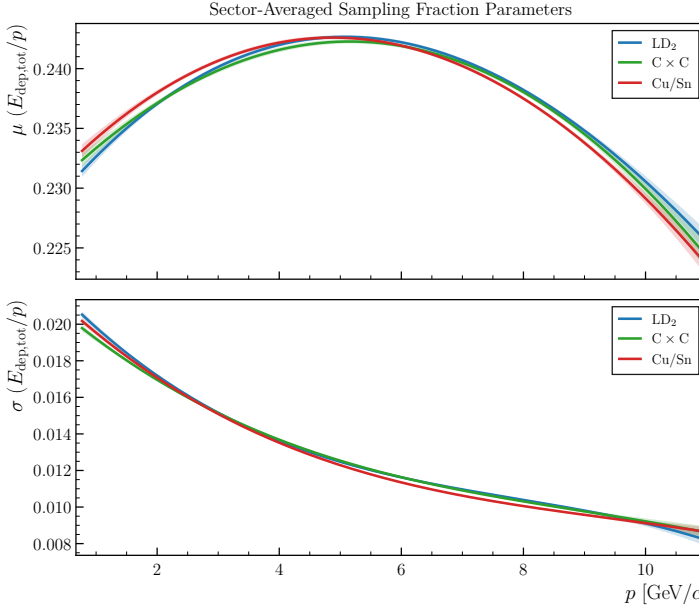


Figure 7. Comparison of the sampling fraction mean and sigma as a function of momentum for all the targets in outbending polarity for the average over all sectors.

119 The sampling fraction behavior also depends on the magnetic field
 120 polarity of the torus. A comparison between inbending (IB) and outbend-
 121 ing (OB) polarities for the LD2 target is shown in fig. 8. Both polarities

exhibit similar sampling fraction mean values and sigma dependencies on momentum, indicating consistent electron identification performance across different field configurations. The slight differences observed are accounted for in the polarity-dependent parameterizations used in the analysis.

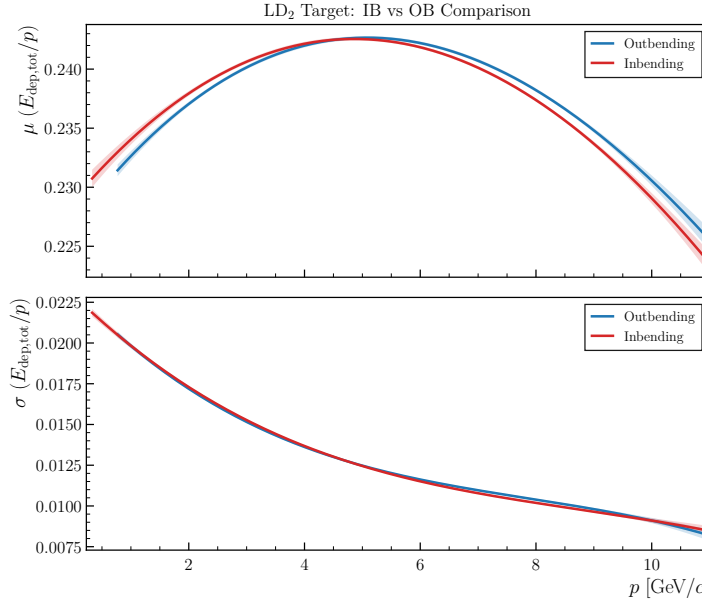


Figure 8. Comparison of the sampling fraction mean and sigma as a function of momentum for the LD2 target between inbending and outbending polarities, averaged over all sectors.

Also, a cut on the momentum of the electron is applied. The cut is defined as $p > 0.8$ GeV. It is applied to remove low-momentum electrons that are known not to be well reconstructed.

The RG-A Common Analysis Note also employed a so-called "triangular" cut. This cut was designed to reduce pion contamination in the electron sample and was developed using the sampling fractions of the preshower calorimeter and the inner calorimeter. However, with our sampling fraction versus momentum cut, DC fiducial cuts, and calorimeter cuts, the pion contamination is already very low, and this cut would remove valid electron tracks. Therefore, this cut is not applied in this analysis. Figure section 1.1 shows the distribution before any refinement cuts (only the pid and status cuts applied), and section 1.1 shows the distribution after all refinement cuts have been applied.

Vertex cuts are applied to ensure that selected electron tracks originate from the target region, thereby reducing background from interactions outside the target. The vertex position along the beamline (V_z) is used to define these cuts.

The V_z distribution for electron candidate tracks in outbending polarity is shown in fig. 10 for the three targets: LD2, CxC, and CuSn. The cuts

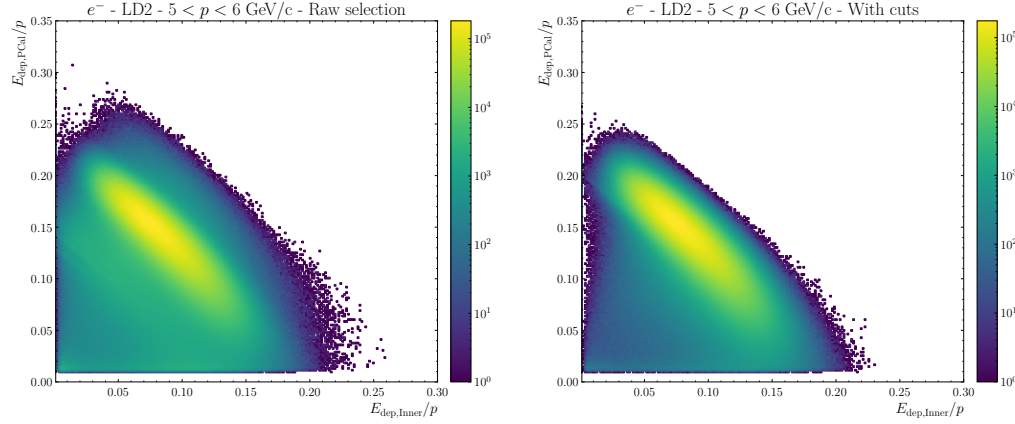


Figure 9. Sampling fraction of the preshower calorimeter vs sampling fraction of the inner calorimeter for electron candidate tracks in the LD2 target in outbending polarity. (a) Before any refinement cuts. (b) After all refinement cuts.

145 were developed by fitting the V_z distributions for the CxC and CuSn targets
 146 with two double-sided Crystal Ball (DSCB) functions for the main target
 147 peaks and two additional DSCB functions for the peaks corresponding to
 148 the empty LD2 cell walls.

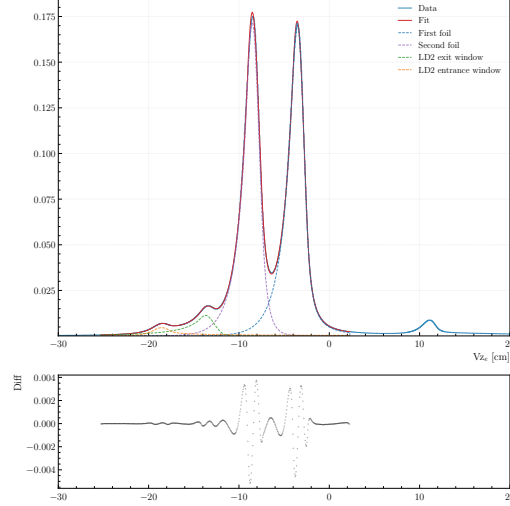


Figure 10. V_z distribution for electrons in outbending polarity for the CxC target, showing the total fit and individual components.

149 For the solid targets, the vertex cut ranges are defined as $\mu \pm 3\sigma$ of
 150 the main peak for each target, where μ is the mean and σ is the standard
 151 deviation. The exception is the upper limit for CxC and Sn, which is set to
 152 5 cm because the next peak corresponds to the scattering chamber windows,
 153 which are sufficiently far from the target region to avoid contamination. For
 154 the LD2 target, the lower limit is set to -15 cm to include the full target

length, and the upper limit is set to 5 cm to avoid contamination from the scattering chamber windows. The resulting vertex cuts for each target in outbending polarity are summarized in table 2.

Table 2. Vertex cut ranges for electron candidates in outbending polarity.

Target	V_z Min (cm)	V_z Max (cm)
LD2	-15.0	5.0
CxC	-10.6	5.0
Cu	-10.6	-6.5
Sn	-5.5	5.0

SUBSECTION 1.2

Electron fiducial cuts

To ensure uniform detector acceptance and reduce edge effects, fiducial cuts are applied to the electron candidates. These cuts define a geometric region within the detector where the response is well understood and consistent. The fiducial cuts are for the drift chambers and the calorimeter.

1.2.1 Calorimeters fiducial cuts

Fiducial cuts for the calorimeters are applied in the local coordinate system of each sector (u , v and w). The RG-A Common Analysis Note provides a detailed description of the calorimeter fiducial cuts, which are implemented here without modification. The cuts are designed to exclude regions near the edges of the calorimeter sectors where the response may be non-uniform or poorly understood. For electron candidates, the fiducial cuts are $v > 9$ cm and $w > 9$ cm. It is done because the PCal bar are 4.5 cm wide, and to have a good clusters formation and reconstruction, the hit should have at least two bars. The profile of the distributions of sampling fraction as a function of v and w for electron candidate tracks in the LD2 target in outbending polarity are shown in fig. 11. Similar plots for the CxC and CuSn targets are available in the appendix. The SF start to drop and fluctuate below 9 cm for both v and w coordinates.

The comparison of the profile of the 2D distribution SF vs v or w for electron candidate tracks in outbending polarity for the three targets: LD2, CxC and CuSn is shown in fig. 12. The three targets present similar distributions and justify the use of the same fiducial cuts.

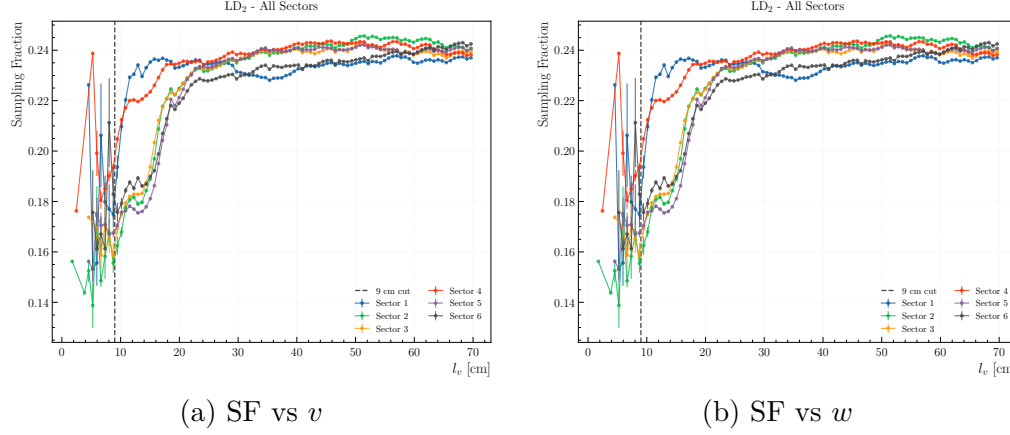


Figure 11. Profile of the 2D distribution SF vs v (a) and w (b) for electron candidate tracks in the LD2 target in outbending polarity for each sector and the overall distribution.

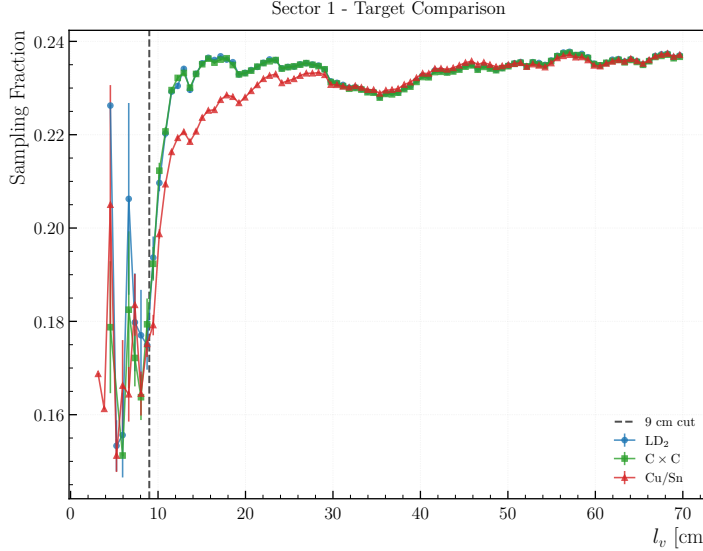


Figure 12. Comparison of the profile of the 2D distribution SF vs v or w for electron candidate tracks in outbending polarity for the three targets: LD2, CxC and CuSn.

1.2.2 DC fiducial cuts

Fiducial cuts for the drift chambers are applied using the local variable `edge` defined in the REC::Traj bank. This variable represents the distance between the virtual edge of the DC (defined in the simulation) and the hit position. To define the cut value, the profile of the 2D distribution of the track χ^2/ndf versus `edge` for electron candidate tracks with outbending polarity is used for the three targets.

The methodology for determining the fiducial cut position is illustrated in fig. 13 and employs a moving variance method. This approach identi-

ties optimal fiducial cut positions by analyzing local stability in the χ^2/ndf distribution as a function of edge distance. The method applies a sliding window (typically 5 points) across the χ^2/ndf profile and calculates the variance within each window. In regions far from the detector edges, where tracking performance is optimal and stable, the χ^2/ndf values exhibit low variance. However, as tracks approach the physical boundaries of the drift chambers, detector inefficiencies and edge effects cause the χ^2/ndf to rise unpredictably, resulting in significantly increased local variance. By scanning from the outer edge inward and identifying the first position where variance exceeds a predefined threshold (typically 0.05), the method systematically determines the boundary between the stable detector region and the degraded edge region. This approach is particularly robust because it captures the transition point where tracking quality begins to deteriorate, rather than relying on arbitrary χ^2/ndf thresholds that may vary across different detector regions or experimental conditions.

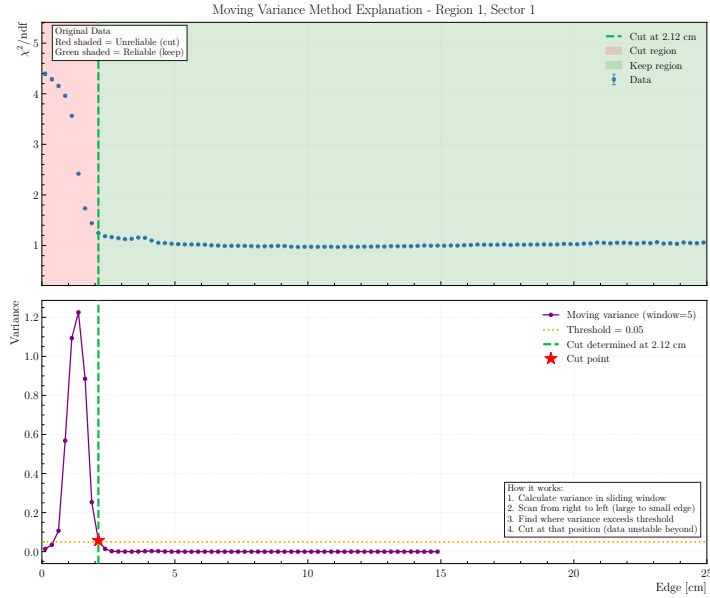


Figure 13. Illustration of the moving variance method used to determine DC fiducial cut positions. A sliding window (typically 5 points) calculates local variance across the χ^2/ndf profile. The method scans from the outer edge inward, identifying the first position where the local variance exceeds the threshold of 0.05, marking the transition from the stable detector region to the degraded edge region.

The resulting fiducial cut for sector 1 and region 1 for the LD2 target is shown in fig. 14a. The same procedure is applied for each sector and each target. The resulting profiles for each sector for regions 1, 2, and 3 are shown in fig. 14b, fig. 14c, and fig. 14d, respectively, for the LD2 target.

To validate the robustness of the DC fiducial cuts, the dependence of the χ^2/ndf profiles on electron momentum and scattering angle is investi-

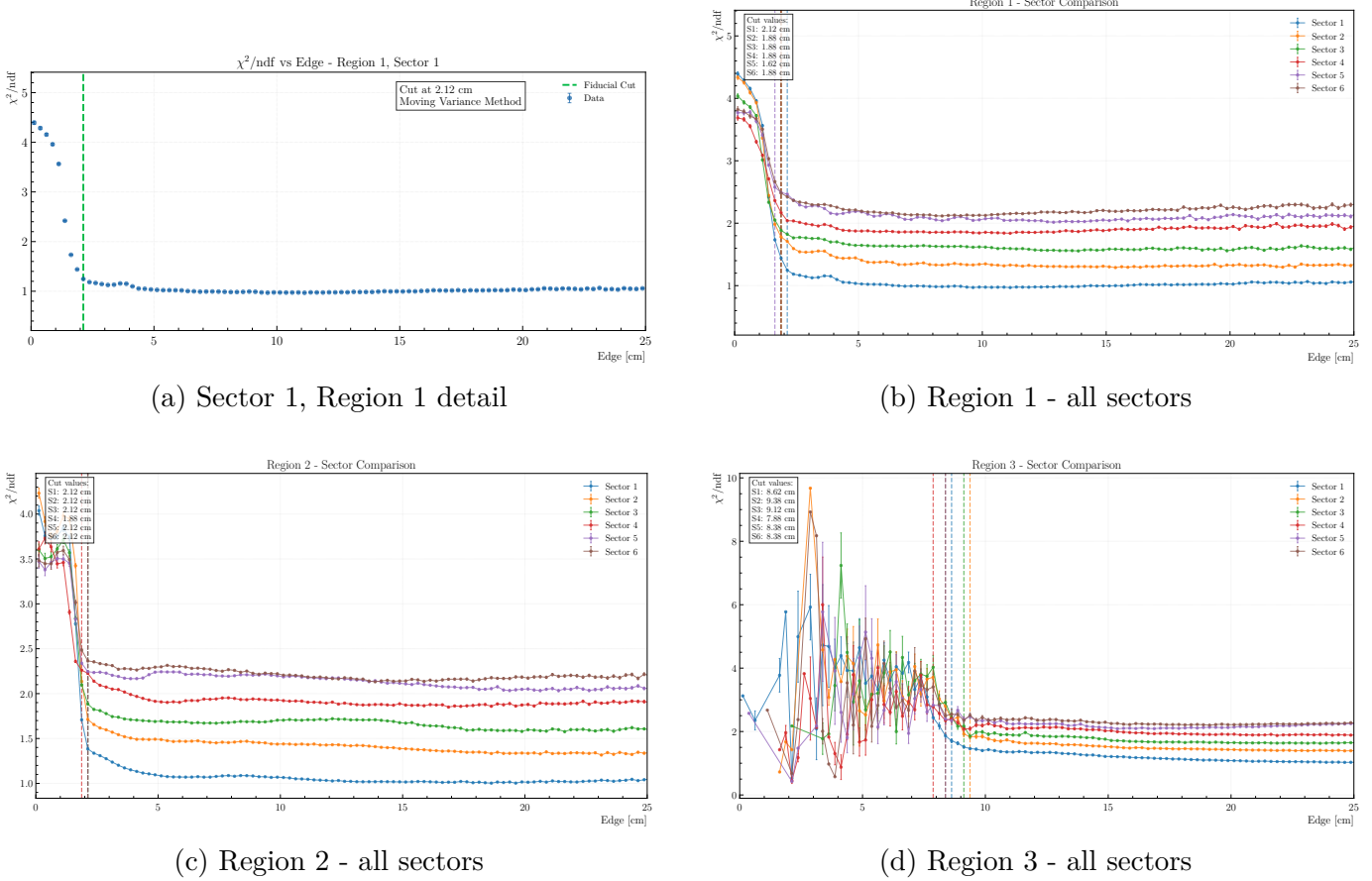


Figure 14. DC fiducial cuts for electron candidate tracks in outbending polarity for the LD2 target. (a) Application of the moving variance method for sector 1, region 1, showing the χ^2/ndf profile with the local variance calculation and the resulting fiducial cut position where variance exceeds the 0.05 threshold. (b-d) Profiles of χ^2/ndf vs edge for all sectors in regions 1, 2, and 3, respectively, with determined fiducial cut positions indicated.

gated. The χ^2/ndf versus edge profiles are examined in different momentum bins (0.5-2 GeV, 2-4 GeV, 4-6 GeV, and >6 GeV) for each region, as shown in figs. 15a to 15c. The profiles remain consistent across momentum ranges, with the fiducial cut positions showing minimal momentum dependence. This indicates that the single fiducial cut value determined from the integrated momentum distribution is appropriate for all electron momenta.

Similarly, the angular dependence is studied by binning the data in polar angle θ ranges corresponding to different detector geometries. As shown in figs. 16a to 16c, the χ^2/ndf profiles exhibit consistent behavior across different θ bins within each region. The slight variations observed are within the statistical uncertainties and do not require θ -dependent fiducial cuts.

The DC fiducial cuts are also compared across the three different tar-

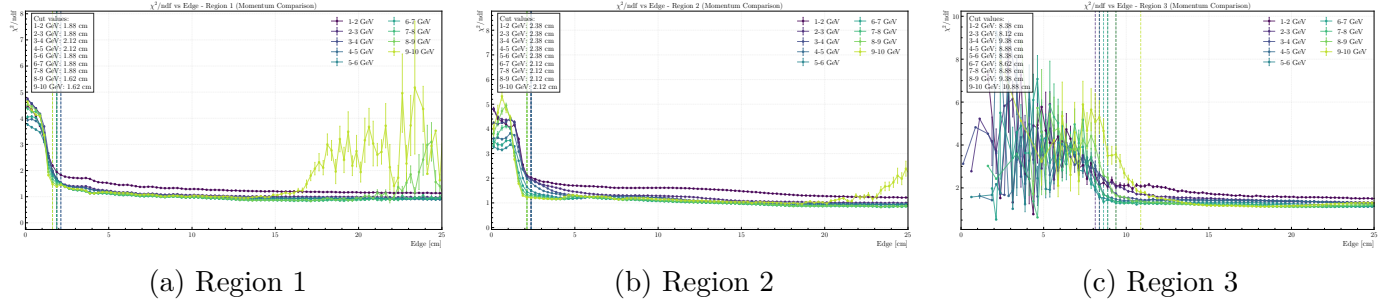


Figure 15. Momentum dependence of DC fiducial cuts for the LD2 target in outbending polarity. The χ^2/ndf vs **edge** profiles are shown for different momentum bins in regions 1, 2, and 3, demonstrating consistent behavior across the full momentum range.

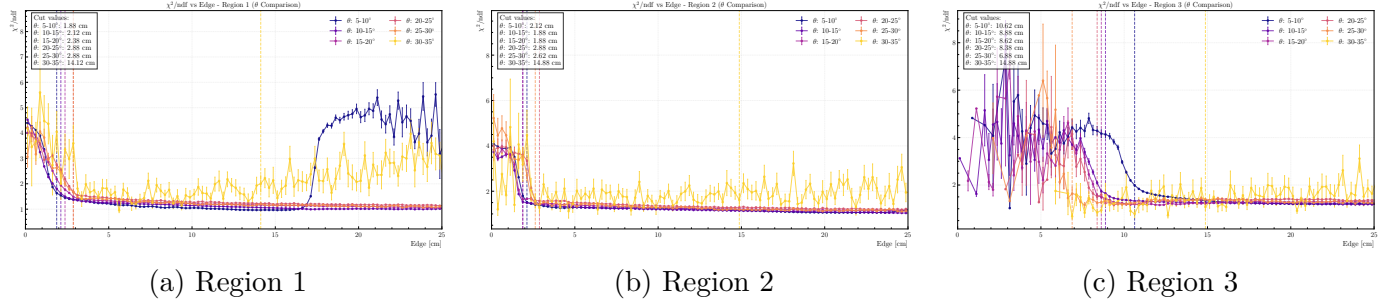


Figure 16. Angular dependence of DC fiducial cuts for the LD2 target in outbending polarity. The χ^2/ndf vs **edge** profiles are shown for different θ bins in regions 1, 2, and 3, showing consistent edge effects independent of scattering angle.

226 gets (LD2, CxC, and CuSn) for sector 1 in each region, as shown in figs. 17a
 227 to 17c. The profiles are nearly identical for all three targets, with fiducial
 228 cut positions differing by less than 0.1 cm on average (see table 3). This
 229 similarity justifies using the same DC fiducial cut methodology across all
 230 targets.

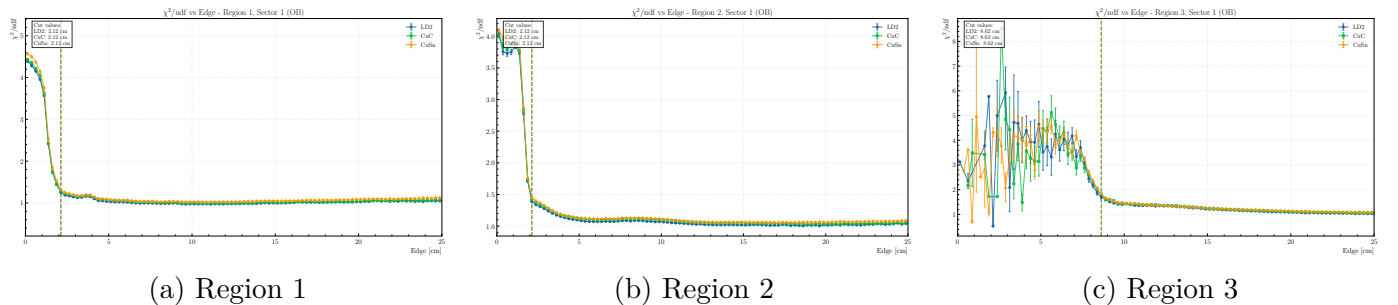


Figure 17. Target comparison of DC fiducial cuts for sector 1 in outbending polarity. The χ^2/ndf vs **edge** profiles for LD2, CxC, and CuSn targets are nearly identical across all three regions, demonstrating target-independent edge effects.

²³¹ The average fiducial cut positions for each region for the outbending
²³² polarity are summarized in table 3.

Table 3. Average Fiducial Cut Positions by Region for the outbending polarity.

Region 1 (cm)	Region 2 (cm)	Region 3 (cm)
1.88 ± 0.16	2.08 ± 0.10	8.62 ± 0.55

²³³ SECTION 2

Summary

Here is a table that recapitulates all the cuts:

Cut Type	Cut Description	Value/Requirement
Particle ID	Event Builder assignment	<code>pid = 11</code> (electron)
Status	Forward Detector trigger	$-4000 < \text{status} \leq -2000$
Momentum	Minimum momentum	$p > 0.8 \text{ GeV}$
SF vs Momentum	Momentum-dependent SF	$\mu_{\text{SF}} \pm 3.5\sigma$ vs p
Calorimeter v, w coordinate	Local coordinate cut	$v, w > 9 \text{ cm}$
Drift Chamber Edge	Distance from DC edge	<code>edge > region dependent</code>
Vertex V_z	Target vertex position	Target dependent (see table 2)

Table 4. Summary of all cuts applied for electron identification and selection in RG-D analysis.

²³⁶
²³⁷ The survival rates after each cut for the different targets are summa-
²³⁸ rized in section 2.

Target	Cut	Cumulative	Step
LD2	Momentum cut	1.0000	1.0000
	Sampling fraction cut	0.9714	0.9715
	PCAL cut	0.9714	1.0000
	DC cut	0.9522	0.9802
	Vz cut	0.8995	0.9447
Cx C	Momentum cut	1.0000	1.0000
	Sampling fraction cut	0.9740	0.9740
	PCAL cut	0.9740	1.0000
	DC cut	0.9550	0.9805
	Vz cut	0.7779	0.8146
CuSn	Momentum cut	1.0000	1.0000
	Sampling fraction cut	0.9824	0.9824
	PCAL cut	0.9823	0.9999
	DC cut	0.9642	0.9816

Table 5. Electron survival rates for different targets

239 SECTION A

240

Sector Parameters

241

242

Outbending (OB)

243

Table 6. Sampling fraction polynomial parameters for outbending polarity.

Target	Sector	a_μ	b_μ	c_μ	d_μ	a_σ	b_σ	c_σ	d_σ
LD2	S1	2.284817E-01	5.741607E-03	-7.956694E-04	2.165831E-05	2.278400E-02	-3.478097E-03	3.644345E-04	-1.564506E-05
	S2	2.272353E-01	6.035907E-03	-5.379217E-04	-1.432191E-06	2.214450E-02	-2.992410E-03	2.810789E-04	-1.021893E-05
	S3	2.248222E-01	9.544562E-03	-1.331928E-03	4.146476E-05	2.455364E-02	-4.547263E-03	5.091026E-04	-2.082045E-05
	S4	2.262726E-01	6.742876E-03	-6.707265E-04	6.027435E-06	2.270259E-02	-3.090211E-03	2.849498E-04	-1.108599E-05
	S5	2.294593E-01	3.253914E-03	-6.716294E-05	-2.106351E-05	2.353437E-02	-4.471507E-03	5.546300E-04	-2.564773E-05
	S6	2.248109E-01	7.709680E-03	-9.387105E-04	1.955346E-05	2.320134E-02	-3.707398E-03	4.086606E-04	-1.827203E-05
CxC	S1	2.297164E-01	4.850482E-03	-6.473612E-04	1.386706E-05	2.160027E-02	-2.804498E-03	2.481187E-04	-9.444168E-06
	S2	2.284924E-01	5.444945E-03	-4.057949E-04	-9.745369E-06	2.097248E-02	-2.301250E-03	1.681611E-04	-4.820942E-06
	S3	2.257831E-01	8.799251E-03	-1.210729E-03	3.520214E-05	2.364466E-02	-3.974250E-03	4.048261E-04	-1.517698E-05
	S4	2.290273E-01	4.774422E-03	-3.194710E-04	-1.291518E-05	2.131817E-02	-2.278156E-03	1.421861E-04	-3.384835E-06
	S5	2.312933E-01	1.779729E-03	-1.881011E-04	-3.479554E-05	2.238608E-02	-3.777670E-03	4.241412E-04	-1.815833E-05
	S6	2.271200E-01	6.051471E-03	-6.286571E-04	1.997614E-06	2.170337E-02	-2.868470E-03	2.639296E-04	-1.041341E-05
CuSn	S1	2.320707E-01	3.994131E-03	-4.894629E-04	1.898325E-06	2.241820E-02	-3.277630E-03	3.136628E-04	-1.234151E-05
	S2	2.302078E-01	3.476050E-03	-1.567172E-04	-2.212723E-05	2.141103E-02	-2.354403E-03	1.075100E-04	1.855098E-06
	S3	2.268107E-01	8.877708E-03	-1.179578E-03	3.071273E-05	2.378785E-02	-4.104492E-03	4.372052E-04	-1.750814E-05
	S4	2.290050E-01	6.702587E-03	-7.847463E-04	1.459749E-05	2.250505E-02	-2.997400E-03	2.528880E-04	-8.680370E-06
	S5	2.298645E-01	4.027068E-03	-2.501636E-04	-1.062495E-05	2.240025E-02	-3.576763E-03	3.577542E-04	-1.355748E-05
	S6	2.268440E-01	6.788151E-03	-8.409054E-04	1.710382E-05	2.268680E-02	-3.427790E-03	3.396480E-04	-1.371903E-05
Average	S1	2.300896E-01	4.862074E-03	-6.441645E-04	1.247456E-05	2.226749E-02	-3.186742E-03	3.087387E-04	-1.247691E-05
	S2	2.286452E-01	4.985634E-03	-3.668113E-04	-1.110160E-05	2.150934E-02	-2.549354E-03	1.855833E-04	-4.394923E-06
	S3	2.258053E-01	9.073840E-03	-1.240745E-03	3.579321E-05	2.399538E-02	-4.208668E-03	4.503779E-04	-1.783519E-05
	S4	2.281016E-01	6.073295E-03	-5.916479E-04	2.569914E-06	2.217527E-02	-2.788589E-03	2.266746E-04	-7.717066E-06
	S5	2.302059E-01	3.020237E-03	-4.307581E-05	-2.216133E-05	2.277357E-02	-3.941980E-03	4.455085E-04	-1.912118E-05
	S6	2.262583E-01	6.849767E-03	-8.027577E-04	1.288497E-05	2.253050E-02	-3.334553E-03	3.374127E-04	-1.413483E-05

244

Inbending (IB)

245

Table 7. Sampling fraction polynomial parameters for inbending polarity.

Target	Sector	a_μ	b_μ	c_μ	d_μ	a_σ	b_σ	c_σ	d_σ
LD2	S1	2.311090E-01	4.309850E-03	-5.451468E-04	4.964926E-06	2.235234E-02	-3.117219E-03	2.887163E-04	-1.130302E-05
	S2	2.304337E-01	3.585701E-03	-1.672183E-04	-2.195166E-05	2.170119E-02	-2.428043E-03	1.302137E-04	-2.341453E-09
	S3	2.269121E-01	8.797654E-03	-1.171428E-03	3.051411E-05	2.423452E-02	-4.301838E-03	4.742717E-04	-1.982933E-05
	S4	2.288870E-01	6.786554E-03	-8.022669E-04	1.557290E-05	2.313618E-02	-3.260224E-03	3.018553E-04	-1.156727E-05
	S5	2.288645E-01	4.637371E-03	-3.662910E-04	-4.233388E-06	2.310886E-02	-3.892809E-03	4.115044E-04	-1.656696E-05
	S6	2.272092E-01	6.581994E-03	-8.197215E-04	1.632205E-05	2.321750E-02	-3.665701E-03	3.804620E-04	-1.587632E-05
CxC	S1	2.311089E-01	4.309932E-03	-5.451631E-04	4.965863E-06	2.235235E-02	-3.117219E-03	2.887137E-04	-1.130271E-05
	S2	2.304337E-01	3.585739E-03	-1.672262E-04	-2.195117E-05	2.170108E-02	-2.427968E-03	1.302009E-04	-1.715883E-09
	S3	2.269124E-01	8.797523E-03	-1.171404E-03	3.051277E-05	2.423476E-02	-4.301797E-03	4.742961E-04	-1.983062E-05
	S4	2.288871E-01	6.786452E-03	-8.022473E-04	1.557178E-05	2.313635E-02	-3.260315E-03	3.018706E-04	-1.156805E-05
	S5	2.288645E-01	4.637396E-03	-3.662963E-04	-4.233103E-06	2.310898E-02	-3.892887E-03	4.115187E-04	-1.656775E-05
	S6	2.272093E-01	6.581935E-03	-8.197067E-04	1.632106E-05	2.321749E-02	-3.665704E-03	3.804646E-04	-1.587659E-05
CuSn	S1	2.311087E-01	4.310017E-03	-5.451781E-04	4.966680E-06	2.235247E-02	-3.117310E-03	2.887315E-04	-1.130379E-05
	S2	2.304337E-01	3.585708E-03	-1.672224E-04	2.195131E-05	2.170126E-02	-2.428101E-03	1.302294E-04	-3.452408E-09
	S3	2.269123E-01	8.797570E-03	-1.171414E-03	3.051337E-05	2.423472E-02	-4.301969E-03	4.742963E-04	-1.983071E-05
	S4	2.288870E-01	6.786555E-03	-8.022665E-04	1.557285E-05	2.313625E-02	-3.260272E-03	3.018643E-04	-1.156777E-05
	S5	2.288646E-01	4.637320E-03	-3.662803E-04	-4.234038E-06	2.310900E-02	-3.892931E-03	4.115288E-04	-1.656837E-05
	S6	2.272092E-01	6.582013E-03	-8.197249E-04	1.632221E-05	2.321744E-02	-3.665649E-03	3.804500E-04	-1.587559E-05
Average	S1	2.311088E-01	4.309933E-03	-5.451627E-04	4.965823E-06	2.235239E-02	-3.117249E-03	2.887205E-04	-1.130317E-05
	S2	2.304337E-01	3.585716E-03	-1.672223E-04	-7.317175E-06	2.170118E-02	-2.428037E-03	1.302147E-04	-2.503248E-09
	S3	2.269123E-01	8.797558E-03	-1.171416E-03	3.051342E-05	2.423467E-02	-4.301928E-03	4.742880E-04	-1.983022E-05
	S4	2.288870E-01	6.786520E-03	-8.022602E-04	1.557251E-05	2.313626E-02	-3.260271E-03	3.018634E-04	-1.156770E-05
	S5	2.288645E-01	4.637362E-03	-3.662892E-04	-4.233509E-06	2.310895E-02	-3.892876E-03	4.115173E-04	-1.656769E-05
	S6	2.272093E-01	6.581981E-03	-8.197177E-04	1.632178E-05	2.321748E-02	-3.665685E-03	3.804588E-04	-1.587616E-05

246 SECTION B

247

Number of photo-electrons in HTCC

248

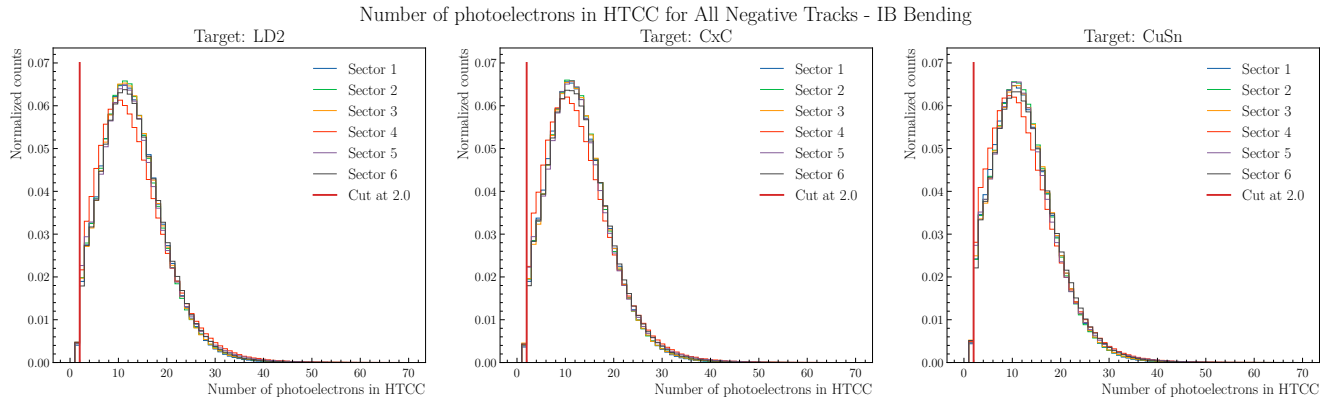


Figure 18. HTCC photo-electron distribution for all negative tracks in the Forward Detector in inbending polarity for the torus, apply cut at $N_{\text{phe}} > 2$ for pion rejection.

249 SECTION C

250

Sampling fraction versus momentum

251

252 SECTION D

253

Calorimeter fiducial cuts

254

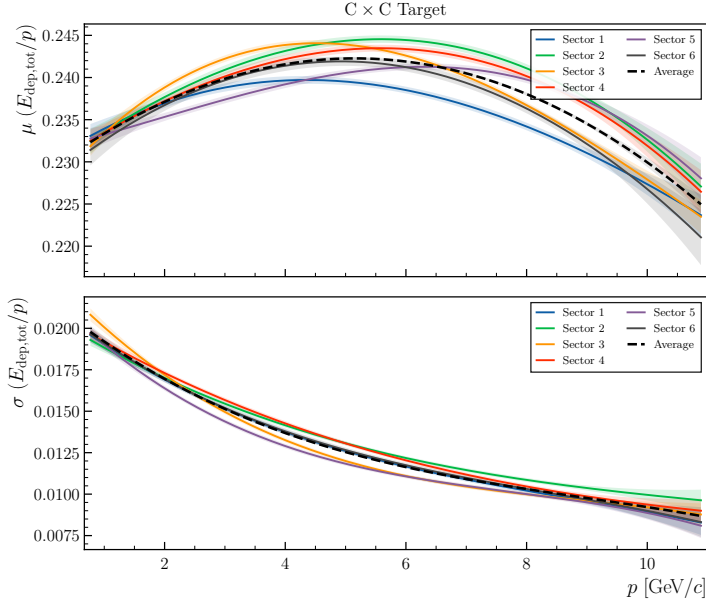


Figure 19. Comparison of the sampling fraction mean and sigma as a function of momentum for the CxC target in outbending polarity for different sectors and the overall distribution.

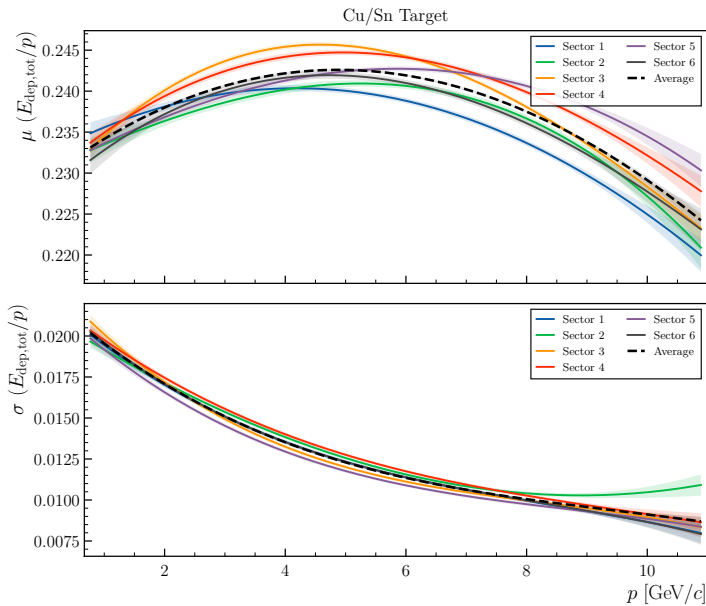


Figure 20. Comparison of the sampling fraction mean and sigma as a function of momentum for the CuSn target in outbending polarity for different sectors and the overall distribution.

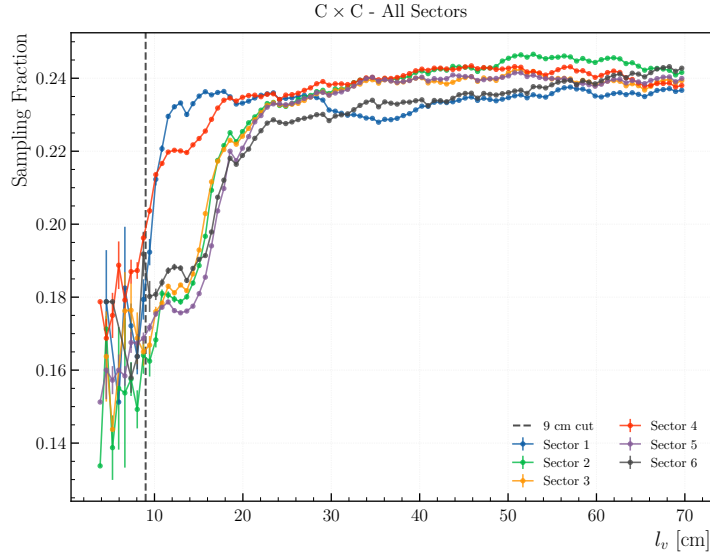


Figure 21. Profile of the 2D distribution SF vs v or w for electron candidate tracks in the CxC target in outbending polarity for each sectors and the overall distribution.

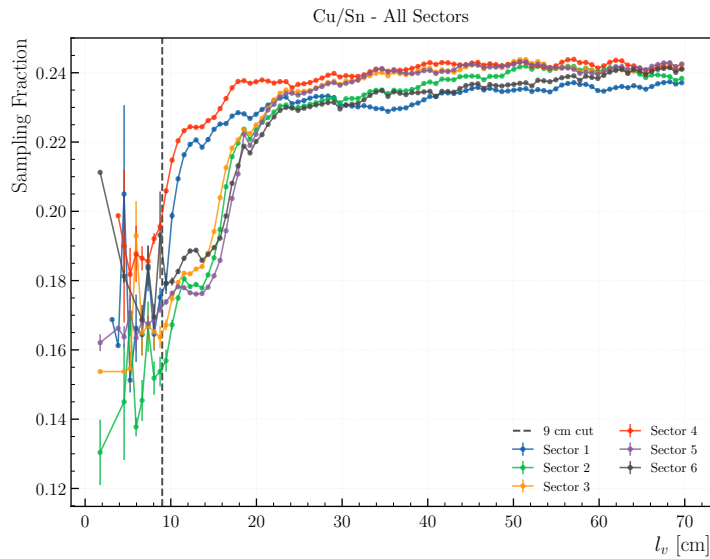


Figure 22. Profile of the 2D distribution SF vs v or w for electron candidate tracks in the CuSn target in outbending polarity for each sectors and the overall distribution.